Lasers in Medical Science
https://doi.org/10.1007/s10103-020-03118-8

ORIGINAL ARTICLE

Dynamic characterization of indocyanine green–assisted dental caries ablation with continuous diode laser using thermal imaging and fluorescence spectroscopy

Mohammad E. Khosroshahi[1,2,3] · Faezeh D. Farahani[1,4] · Lida Ghazanfari[1,5] · Vaughan Woll-Morison[2]

Received: 7 May 2020 / Accepted: 1 August 2020

Abstract
We describe the time-resolved thermal changes in indocyanine green (ICG)–assisted diode laser ablation of dental caries as a potential technique for painless treatment based on the selective photoabsorption and controlled photothermal ablation. Static ablation mode produced a higher temperature rise compared with scanning mode due to localized accumulation of heat. A temperature rise between 45–80 and 70–95 °C was obtained after 20 s that corresponded to 29 and 80 W cm^{-2}, respectively. The temperature of the tooth surface increased by irradiation time, and it behaved linearly up to 70 °C at 29 and 80 W cm^{-2}. A maximum ablation per area of about 0.3 and 0.45 mg cm^{-2} was achieved after 80 s exposure at 29 and 80 W cm^{-2}, respectively. A statistically significant difference is observed in mean carious teeth weight at various exposure times between low and high irradiances. A thermal penetration depth of 0.8–9 mm is determined for 1–100 s of exposure time. The IR thermal imaging of ICG temperature as a function of exposure time showed a linear increase for 60 s beyond which it deviated. The laser-induced fluorescence spectroscopy indicated that the ICG quality can be altered during the course of irradiation, which in our case, it corresponded to ≈ 78% loss of signal within 23 min of exposure. The caries removal experiment was performed within 100 s corresponding to ≈ 7% loss. We believe that the application of the above-combined technique can be utilized as a monitoring device to control the ablation interaction process.

Keywords Dental caries · Diode laser · Indocyanine green · Thermal response · Thermal imaging · Fluorescence spectroscopy

Introduction

Dental caries is the most prevalent chronic infectious disease, which arises from an overgrowth of specific bacteria that can metabolize fermentable carbohydrates, hence producing acids as waste products of their metabolism. The dentinal lesion consists of two distinct layers with different ultrastructural and chemical characteristics. When the outer layer is contaminated with bacteria, the matrix significantly degrades and it cannot be remineralized. But the inner layer, which is not contaminated with bacteria, partially becomes demineralized [1]. Caries can be described as a process resulting in structural changes to the dental hard tissue, and its onset normally is characterized by microscopically visible surface demineralization on dental tissue, but visual inspection presents lower sensitivity and is subjective. In this regard, extensive research has been done in two particular directions of diagnosis and removal.

In the former case, it is important that hidden caries be diagnosed at early stages so that appropriate preventive and restorative treatment can be applied promptly. Some of the applied techniques include the following: plasma spectroscopy (PS) [2–5], polarized Raman spectroscopy (PRS) [6], light scattering [7], optical coherence tomography (OCT) [8], fibre-delivered confocal microscopy (FCM) [9, 10], quantitative

✉ Mohammad E. Khosroshahi
m.khosro@miselectronics.com; khosrom@mie.utoronto.ca

[1] Laser & Nanobiophotonics Laboratory, Faculty of Biomedical Engineering, Amirkabir University of Technology, Tehran, Iran

[2] Nanobiophotonics & Biomedical Research Laboratory, MIS-Electronics Inc., Richmond Hill, Canada

[3] Department of Mechanical and Industrial Engineering, University of Toronto, Toronto, Canada

[4] Medric Teb Co., Tehran, Iran

[5] Eshelman School of Pharmacy, University of North Carolina-Chapel Hill, Chapel Hill, NC, USA

Published online: 08 August 2020

light fluorescence (QLF) [11–13], photothermal radiometry (PTR) [14], photothermal imaging (PTI) [15], near IR imaging (NIRI) [16] and diagnodent laser fluorescence (DLF) [17, 18].

Over the decades, a variety of lasers have been used in research and clinical practice in dentistry due to less pain compared with the mechanical high-speed drilling process, selective tissue removal, analgesic and inflammatory effects and also the benefit of more cost-effective treatment. These lasers mainly include CO_2 (carbon dioxide) 10.6 μm [19], Ho:YAG (holmium:yttrium aluminium garnet) (2.1 μm) [20] and Nd:YAG (neodymium:yttrium aluminium garnet) (1.06 μm) [21] which have indicated evidence of cracking, melting, fissuring and charring on enamel, pulp and dentin tissues. However, laser such as Er:YAG (erbium:yttrium aluminium garnet) (2.94 μm) [22] with maximum peak absorption in water, Er:YSGG (erbium:yttrium scandium gallium garnet) (2.79 μm) [23] and HF (hydrogen fluoride) (2.75–2.94 μm) [2] wavelengths match the absorption peak of hydroxyapatite produce relatively cleaner cuts and ablation.

Ultrashort lasers have shown to produce considerably less thermal and mechanical damage compared with longer pulse duration [24]. Despite this, in most clinical cases, focusing and high power are required for ablation, which normally leads to a rapid tooth superficial temperature rise and hence heating the layers beneath. It has recently been demonstrated that high power pulsed laser ablation of dental materials such as normal tissue, caries and amalgam can produce a significant amount of photoacoustic pressure and plasma-induced temperature, which increases with laser fluence [5]. However, it is noteworthy that the thermal and acoustic transients and hence the physical effects depend on how weak or strong absorbing is the material, which in turn determines whether it is thermally thick or thin and optically transparent or opaque. It is this condition that governs the degree and location (i.e. surface or bulk) of possible microstructural damage caused during the process of laser interaction.

It has been shown that indocyanine green (ICG-C43H47N2NaO6S2) with an absorption band between 600 and 900 nm and a peak around 810 nm can be a potential alternative to efficiently remove dental caries [25–29] and perform soft tissue soldering to reduce the thermal and mechanical side effects [30, 31]. Its mechanism is based on the selective photoabsorption of 810 nm diode laser wavelength where ICG shows an absorption band between 600 and 900 nm, which results in localized heat deposition at the site of action, thus confining the energy penetration in a small volume [25]. Therefore, the risk of thermal damage to the surrounding hard and soft tissues is reduced because ICG has the advantage of binding well to proteins and water, which tends to bind to caries rather than to the surrounding healthy tissue where they absorb poorly the near-infrared light [25, 27, 31]. Hence, the requirement for precise focusing and aiming of the laser beam may be neglected. The goal of this work was to study the time-resolved thermal characteristics of dental caries ablation using a continuous diode laser and an infrared absorbing agent (i.e. ICG) and, also, to monitor the quality of ICG during the ablation process by laser-induced fluorescence spectroscopy and thermal imaging.

Materials and methods

Altogether, twenty carious mandibular premolars, molar (wisdom) and incisor samples with age ranging between 20 and 40 that were extracted for different reasons were provided and categorized by the Tehran Medical University, Faculty of Dentistry. The samples were collected on the same day of extraction or on the following day. Immediately after extraction, they were cleared of food particles lesions or blood clots using a toothbrush under running tap water and stored in 10% formalin at room temperature prior to their sterilization by 1% hypochlorite. The samples were then preserved in deionized water for 1 day before the experiment. To ensure that the change in measured mass is due to the ablation and not due to the dehydration, the samples were placed inside a dry (Ohaus, H-4737) oven on the paper filter for 4 h at 37 °C to dry before laser irradiation; no difference in mass measurement was observed between before and after drying.

Experiment

Prior to the experiment, the absorbance of ICG was measured by UV-Vis spectrometer (Cole-Parmer-Canada). A home-built tunable CW 1.5–6 W diode laser with peak emission at 810 nm with a linear beam profile with dimensions of $1 \times 7\ mm^2$ was used to irradiate the samples at various irradiances. ICG sodium salt is normally available in powder form and can be dissolved in various solvents; 5% (< 5% depending on batch) sodium iodide is usually added to ensure better solubility. Based on our previous experience, 0.25 mg of ICG was mixed with 1 ml of deionized water to prepare the dye solution source from which about 100 $\mu g\ ml^{-1}$ was applied on the sample surface using 1 ml disposable tuberculin needle as shown in Fig. 1.

Two modes of static and dynamic (i.e. scanning) were tested to compare the results. In the former case, the laser spot irradiated a new position at the surface, whereas in the latter, a stepper motor scanned the laser probe on the surface. The ablation experiment was performed in the static mode. An air-water spray was used to clean the irradiated surface. A digital K-type thermometer (CHY502A1, CHY Firemate Co., Taiwan) was positioned directly at the surface to measure the temperature variation. The temperature was measured once per second using CHY recording software. The initial mass of the tooth before (m_i) and after the dry oven (m_d) and

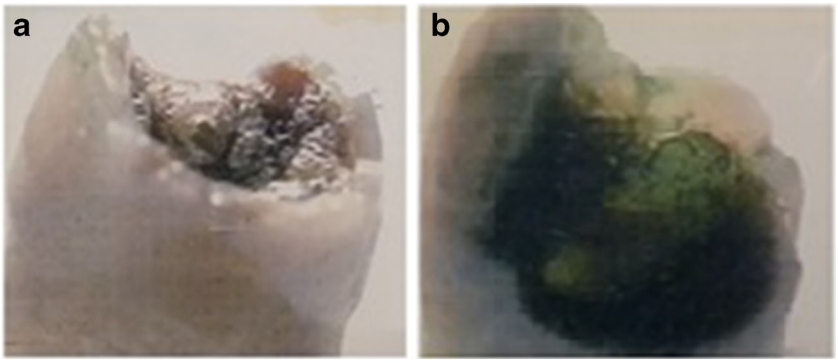

Fig. 1 An example of a carious tooth before and after applied ICG chromophore

laser exposure (m_l) was measured using a sensitive scale; the total mass removed (m_f) was calculated as $m_f = m_d - m_l$. A new sample was used for measurement of temperature at various exposure times and irradiances. The images were recorded by a fast CCD camera (Panasonic Super Dynamic WV-CP450) connected to an optical microscope (Prior-UK). The fluorescence of ICG was recorded via a 500 μm core diameter optical fibre to UV-Vis spectrometer (USB 2000, Ocean Optics) equipped with 2048-pixel linear silicon CCD array (14 μm × 200 μm) with a detector range of 200–850 nm and an optical resolution of 1.5 nm (full-width half maximum) FWHM, where it was then analysed by a computer. To monitor the thermal response of ICG alone, a clear PVC tube with a dimension of 10 × 2 mm was filled with 1 ml of solution and irradiated at constant irradiance of 29 W cm^{-2} at the perpendicular direction, and the corresponding temperature was measured by a thermal camera (Fluke- PTi120-Canada). In this way, the gradual heat distribution with exposure time within ICG was easily monitored.

Results

Figure 2a shows the absorbance peaks of ICG at 720 and 780 nm where the latter is very close to the laser wavelength. Initially, the thermal response of the sample was studied as a function of time at different irradiances where a new position was irradiated in each case. As it is seen in Fig. 2b, the temperature of the surface increases linearly with exposure time and the irradiance. The temperatures of about 46 °C and 82 °C were achieved at 29 W cm^{-2} corresponding to 20 and 100 s irradiation time, and it increased to between 70 and 90 at 80 W cm^{-2} and above 100 at about 160 W cm^{-2} for the same period of exposure.

Time-resolved temperature dynamic in static mode at constant irradiance of 29 and 80 W cm^{-2} is illustrated in Fig. 3a where the curve in both cases initially behaves linearly for nearly 20 s where it approaches the turning point and the temperature continuous increasing reaching 80 °C and 90 °C at 29 and 80 W cm^{-2}, respectively. However, in the scanning mode, the temperature was much lower than the static mode likely because of lower thermal accumulation and rapid heat sink due to ohmic loss and conductivity. The effect of the number of scans on temperature rise at a constant value of 80 W cm^{-2} shows that on average the temperature reaches to about 30 (Fig. 3b), 40 (Fig. 3c) and 35 °C (Fig. 3d) after 6, 14 and 18 scans, respectively. This might be due to complete evaporation of the ICG layer after a defined number of scans, and the laser beam makes direct contact with the tooth surface.

The average of ablation per area for three samples after irradiation was calculated as described above, and the results are shown in Fig. 4a, where at 29 W cm^{-2}, the ablation increases linearly up to 60 s after which it deviates from linearity

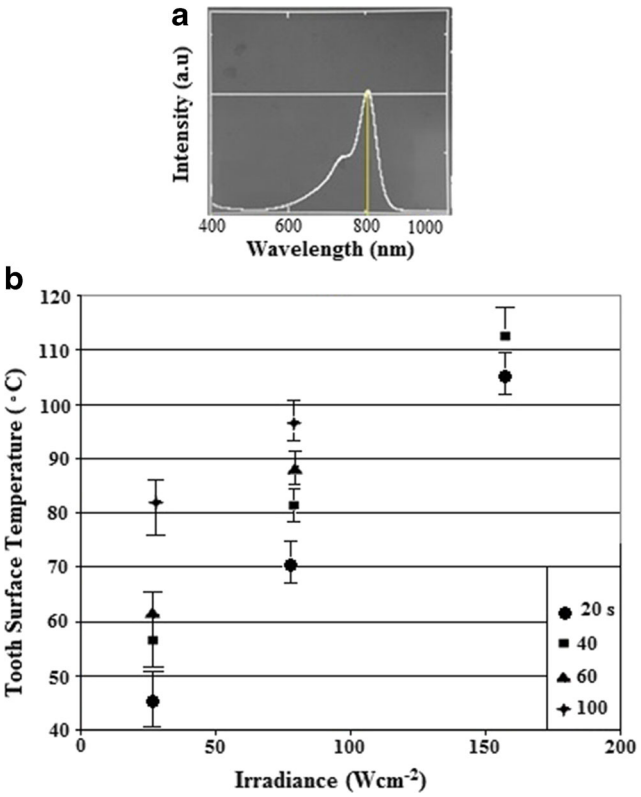

Fig. 2 **a** Absorbance of ICG with a peak around 800 nm. **b** Variation of tooth surface with irradiance at various exposure time

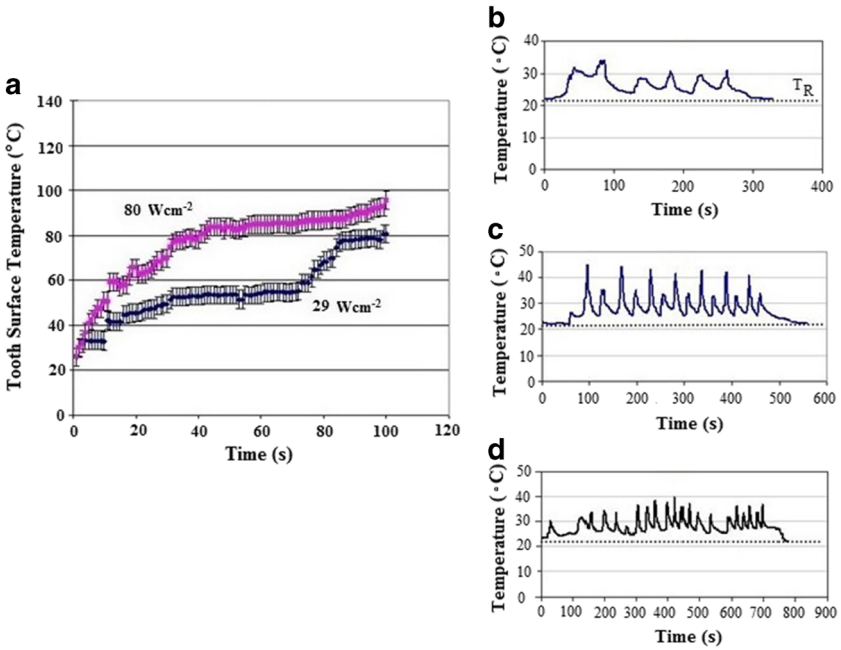

Fig. 3 Time-resolved measurement of carious tooth surface temperature with time at various irradiances: **a** static at 29 W cm^{-2} and **b** 14, **c** 16 and **d** 18 scans at 80 W cm^{-2}, respectively

due to non-linear coupling mechanisms of light propagation, thermal, material and hydro-responses. It is known that the dynamic variation of optical properties with temperature can change the optical response of material such as tissue with laser irradiance [32, 33]. At 80 W cm^{-2}, the ablation rate is considerably higher and increases linearly with the exposure time. A statistically significant difference can be seen in mean carious teeth weight at various exposure times between low and high irradiances. The ablation of carious lesions is via ICG preferential binding to caries rather than to the healthy tissue, and therefore, the laser selectively removes the dye caries combination. The temperature variation with ablation is indicated in Fig. 4b, where at 29 W cm^{-2}, the temperature behaves linearly up to 40 s corresponding to about 65 °C and then deviates at higher exposure time due to stronger evaporation and reaching to about 76 °C after 80 s with maximum ablation rate of 0.31 mg cm^{-2}. However, at a higher value of 80 W cm^{-2}, a sharp rise of temperature after 40 s was observed exceeding 95 °C corresponding to about 0.47 mg cm^{-2} after 100 s irradiation.

At this stage, an independent experiment was performed to study the ICG quality during the ablation and its temperature variation with exposure time at constant irradiance of 29 W cm^{-2}. Typical radial temperature profiles of the ICG tube during the heating are presented in Fig. 5a–h, and as seen in Fig. 5i, the temperature increase exhibits a non-linearity after 60 s and it reaches to about 105 °C after 100 s. After this, the temperature remained almost constant and the laser was switched off allowing the ICG to gradually cool down. This confirms that within the acceptable experimental error of about 10% between contact and non-contact measurements, the results are very closely related and that the ICG was not completely evaporated within a short period.

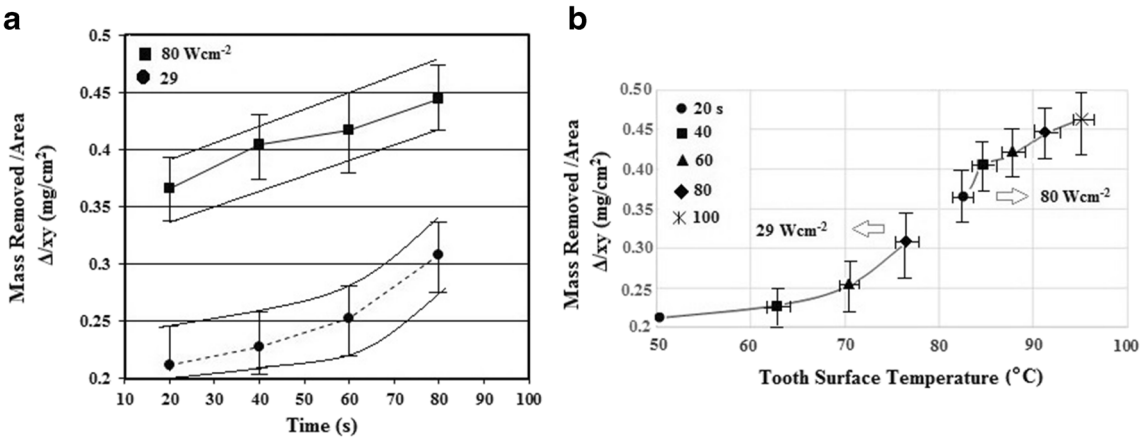

Fig. 4 **a** Variation of average mass removal per area with time at different irradiances. **b** The corresponding temperature rise at the surface

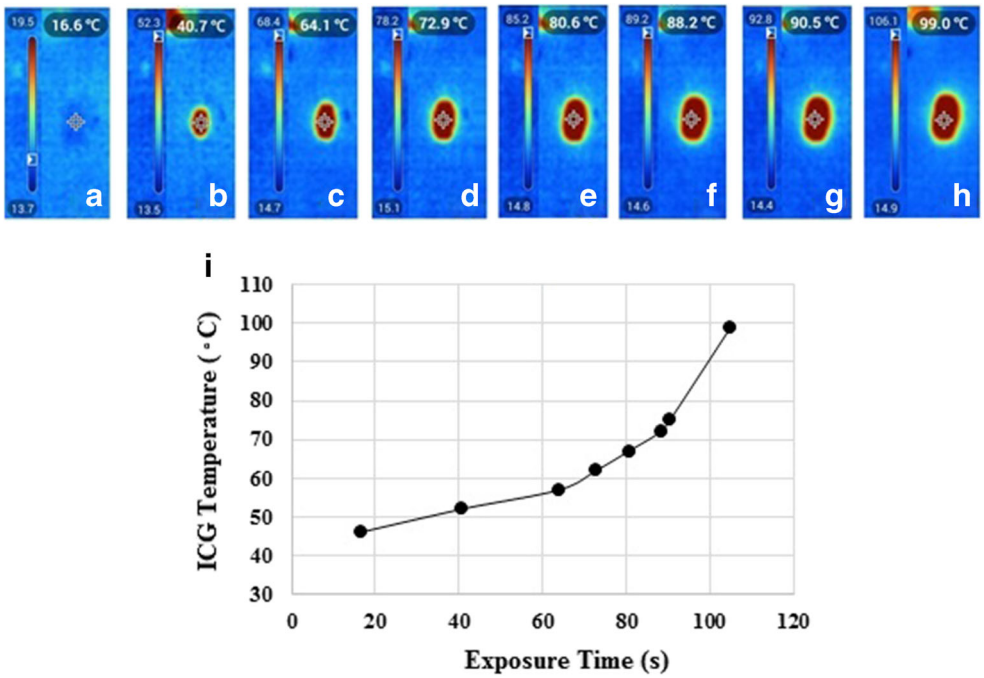

Fig. 5 **a**–**h** The IR thermal images of temperature rise of ICG with diode laser irradiation time and **i** the corresponding plot of **a**

However, it was shown that at longer exposure time, its chemical property gradually changes. As seen in Fig. 6, the time-resolved laser-induced fluorescence signals slowly decrease with exposure time losing about 78% of its fluorescence within 23 min. Since, in our case, the experiment was performed within 100 s, this corresponds to ≈ 7%, which can be assumed negligible, and thus, no significant change could affect the results. It is noteworthy that ICG has a half-life of 150 to 180 s in the body, which is then removed from circulation exclusively by the liver.

Figure 7 demonstrates microscopic images of decay ablation at various irradiances and irradiation times where Fig. 7 (a, b) and (c, d) correspond to before and after ablation using 20 and 100 s exposures at 29 W cm^{-2}, respectively, and the corresponding results for 80 W cm^{-2} are shown in Fig. 7 (e, f)

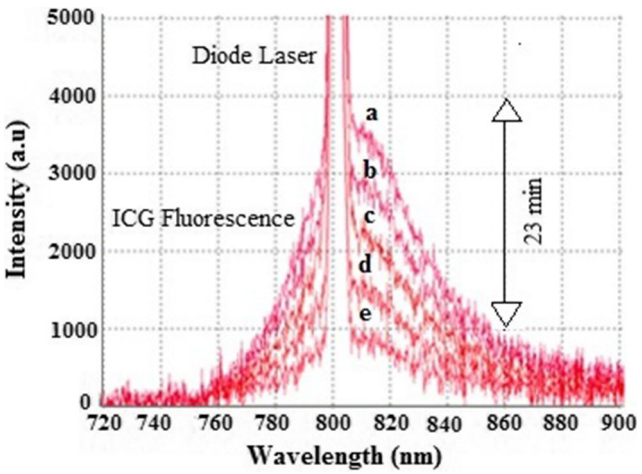

Fig. 6 The laser-induced fluorescence spectra of ICG as a function of irradiation time. Note a gradual decrease of intensity from **a** to **e** due to thermal effects corresponding to 73% within 23 min

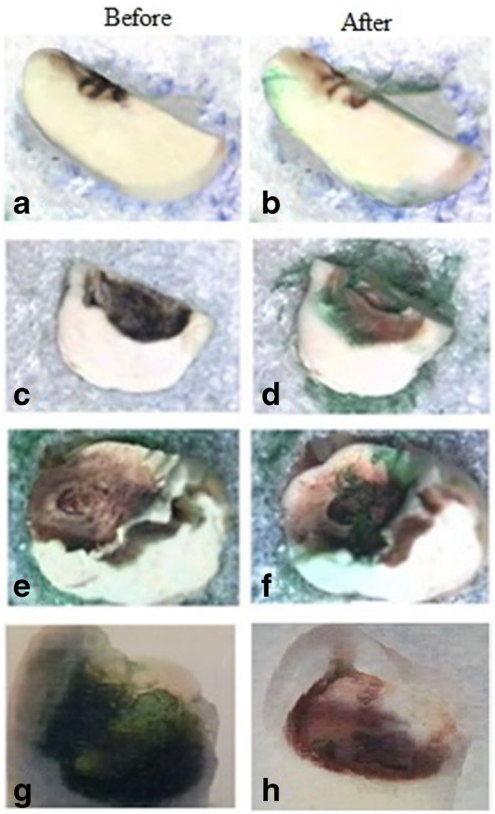

Fig. 7 Microscopic images of teeth samples (a, b) and (c, d) corresponding to before and after ICG-assisted caries removal for 20 and 100 s irradiation time at 29 W cm^{-2}, respectively, and (e, f) and (g, h) represent the corresponding results at 80 W cm^{-2}

and (g, h). Clearly, as the irradiance and the irradiation increase, cleaner results are obtained, but at the same time, the temperature also increases which needs to be optimized. This is due to ICG preferential penetration in caries where it strongly binds with water and protein content (Fig. 7).

Discussion

The chromophore-assisted (i.e. ICG) ablation offers a potential technique for removal of dental caries; however, the dynamic of temperature profile during the operation should be considered to prevent excessive thermal damage and also monitor the ICG quality. The concepts of wavelength-dependent tissue absorption, optical penetration depth and thermal relaxation time allow a rational selection of laser wavelengths and define the exposure conditions. These parameters can be chosen and optimized so that minimal tissue injury is provided. The idea of the concept of selective photothermolysis was introduced by Anderson and Parrish [34].

The advantage of this technique is that the energy is selectively absorbed and deposited in the target area in a controlled manner and that there may not be a need for precise focusing and aiming of the laser beam. Because of increased absorption characteristics of the dyed tissue, lower irradiances may be used to achieve the required effect. When the laser radiation interacts with ICG, the selective absorption of energy is transformed into heat acting as a heat source within the medium. The subsequent temperature rise in the ICG is conducted to caries underneath leading to its ablation via vaporization and possibly pyrolysis of macromolecules. At the ablation or near ablation threshold, heat is deposited at the surface as the heat of ablation H_a (J kg^{-1}) and the energy balance at the ablation front position in 1-D is

$$K\frac{\partial T}{\partial z} = \rho H_{ab}\frac{dx}{dt} \tag{1}$$

So, a positive ablation velocity (dx/dt) should have a positive temperature gradient ($\partial T/\partial z$) and a net heat flow to the surface of the sample according to Fourier's law of heat transfer. The spatial distribution of this heat source is directly related to a number of factors including the profile of heat source, the optical properties of the medium (i.e. absorption and scattering) and the magnitude of heat produced. The temperature field is governed by the time and space-dependent Fourier parabolic heat equation

$$\rho c\frac{\partial T(x,t)}{\partial t} = K\nabla^2 T + Q(t) \tag{2}$$

where $T(r,t)$ (K) is the temperature, $t(s)$ is time, ρ is the density (kg m^{-3}), c is the specific heat capacity (J kg^{-1} K^{-1}), K (W m^{-1} K^{-1}) is the thermal conductivity, $Q(r,t) = I\alpha = P/V$ is the amount of heat deposited per unit volume, I is the laser irradiance (W cm^{-2}), α is the absorption coefficient (cm^{-1}), P is laser power (W) and V is the volume (cm^3). The temperature due to heat deposition is defined by

$$T(r,t) = \frac{\alpha}{\rho c_p}\int_0^t Idt \tag{3}$$

But the dynamics of optical properties such as absorption coefficient changes during the course of heating at constant irradiance; thus, the change of temperature with depth is defined in terms of absorption coefficient as a function of time.

$$\frac{\partial T(r,t)}{\partial z} = \frac{I}{\rho c_p}\int_0^t \frac{\alpha dt}{\partial z} \tag{4}$$

At the ablation threshold, the heat deposited at the surface is expended as the heat of ablation, i.e. the heat due to irradiance, $q_\rho(r) = V_i\, q_\rho(r)\, d^3r$, where the integral is over ICG volume, V_i, and the heat deposited deeper within caries is used to increase the temperature. Assuming that the scattering coefficient of ICG at ≈ 810 nm is negligible compared with its absorption coefficient (i.e. $\alpha >> \beta$), then 85% of incident laser energy is absorbed within twice the optical penetration depth, d_0, of material. For 0.25 mg ml^{-1} ICG at 810 nm, $\alpha \approx$ 117 cm^{-1}, which gives an optical penetration depth of $d_0 \approx \alpha^{-1} \approx 85$ μm [35], and the heat delivered per unit volume of ≈ 3.4–9.4 W mm^{-3} for corresponding irradiances, respectively. Assuming the values of density, $\rho \approx 1.7$ g cm^{-3}, thermal conductivity $K \approx 0.0056$ W cm^{-1} °C^{-1} and specific heat capacity ≈ 3.4 Js^{-1} °C^{-1} for ICG, thermal diffusivity can be calculated by $k \approx K/\rho C \approx 1.53 \times 10^{-3}$ cm^2 s^{-1}. Thus, the thermal relaxation time within ICG is defined and given by using $\tau_r \approx d_0{}^2/k \approx 1.2$ ms. Thus, a thermal penetration depth of $X_T \approx (4kt)^{1/2} \approx 0.8$–9 mm is determined for 1–100 s of exposure time.

This result suggests that longer irradiation time, which gives a thermal depth in order of few millimetres may not be recommended due to proximity of heat transfer to soft and sensitive pulp region. Therefore, the laser deposition and subsequently the heat conduction and temperature rise within the tissue will determine the final effect on the tooth and hence the extent of morphological changes. The final temperature profile will be a function of tissue configuration, beam size, dye concentration and exposure time. The IR thermal imaging of ICG temperature as a function of exposure time provided useful information about heat distribution and that it exhibited a non-linear behaviour. Interestingly, the curve was linear for about 60 s similar to Fig. 4a, where the mass removal became non-linear.

This may suggest that the onset of non-linearity, for given reasons, at a particular exposure time plays a role in the

removal rate due to changes in the interaction process, which is briefly mentioned above. The laser-induced changes in fluorescence of ICG demonstrated a series of linearly decreasing signals by time, which is indicative of some alterations in ICG quality occurring in the process of heating. This can be taken as an advantage to monitor online the laser-caries interaction process where the reduction of peak intensity can represent the time for loss of ICG quality and consequently the changes in the ablation rate. In this case, a loss of 7% was estimated for a total of 100 s irradiation before any significant changes take place in intensity.

Conclusions

The ICG-assisted diode laser ablation of dental caries technique can offer a potential alternative to non-dye laser ablation and the mechanical drill as a painless treatment due to selective and controlled photothermal ablation. Thermal side effects due to the temperature rise in the dental pulp can be controlled by the laser power, exposure time and the dye concentration used. Thus, minimum thermal damage is expected to the surrounding hard and soft tissues determined by thermal penetration depth. Increasing the irradiance increases the tooth surface temperature, which also increases linearly with exposure time. Static ablation mode produced a higher temperature rise due to the localized accumulation of heat. In practice, an external cooling system can be used to reduce the possible excess thermal effect on the surrounding area. The thermal imaging and fluorescence results provided some useful practical online information, which can be utilized to monitor the quality of ICG during the laser interaction process.

Acknowledgements The authors would like to thank Tehran Medical University, Faculty of Dentistry, for providing the teeth samples and also greatly acknowledge the contribution and support of Biomedical Research Lab., MIS Electronics Inc., where the ICG fluorescence spectroscopy and thermal imaging experiments are performed.

Funding information The ablation experiment was performed in Laser & Nanobiophotonics Lab. of Faculty of Biomedical Engineering at AUT under Faculty Grant Program; the spectroscopy and imaging experiments were supported by Nanobiophotonics & Biomedical Research Lab. at MIS Electronics Inc.

Compliance with ethical standards

Conflict of interest The authors declare that they have no conflict of interest.

Ethical approval This research does not contain any form of studies with human participants or animals performed by any of the authors.

References

1. Hosoya Y, Taguchi T, Tay F (2006) Evaluation of a new caries detecting dye for primary and permanent carious dentin. J Dent 35: 137–143. https://doi.org/10.1016/j.jdent.2006.06.004
2. Khosroshahi ME, Ghasemi A (2004) Interaction studies of multimode pulsed HF laser with enamel tissue using photothermal deflection and spectroscopy. Lasers Med Sci 18:196–203. https://doi.org/10.1007/s10103-003-0283-5
3. Thareja R, Sharma A, Shukla S (2008) Spectroscopic investigations of carious tooth decay. Med Eng Phys 30:1143–1148. https://doi.org/10.1016/j.medengphy.2008.02.005
4. Neimz M (1994) Evaluation of physical parameters during the plasma-induced ablation of teeth. Proc SPIE 2323:170–179
5. Khosroshahi ME, Valyzadeh S (2020) Measurement of pulse Nd: YAG laser-induced stress and analysis of dental tissue and amalgam plume using uniaxial polyvinylidene fluoride-based photoacoustic sensor and plasma spectroscopy. Opt Laser Technol 128: 106–239. https://doi.org/10.1016/j.optlastec.2020.106239
6. Ko A, Hewko M, Sowa M, Cleghorn B (2006) Detection of early dental caries using polarized Raman spectroscopy. Opt Express 14: 203–221. https://doi.org/10.1364/OPEX.14.000203
7. Schneiderman A, Elbaun M, Shultz T (1997) Assessment of dental caries with digital imaging fiber-optic trans illumination: in vitro study. Caries Res 31:103–107. https://doi.org/10.1159/000262384
8. Popesca D, Sowa M, Hewko (2008) Assessment of early demineralization in teeth using the signal attenuation in optical coherence tomography images. J Biomed Opt 13:054053. https://doi.org/10.1117/1.2992129
9. Kimura Y, Wilder P, Krasiova T, Anna Maria A Visualization and quantification of healthy and carious dentin structure using confocal laser scanning microscopy. Proc SPIE 2672:64–72. https://doi.org/10.1117/12.238754
10. Rousseau C, Poland S, Girkin J (2007) Development of fibre-optic confocal microscopy for detection and diagnosis of dental caries. Caries Res 41:245–251. https://doi.org/10.1159/000101912
11. Hall A, Deschepper E, Ando M (1997) In vitro studies of laser fluorescence for detection and quantification of mineral loss from dental caries. Adv Dent Res 11:507–514. https://doi.org/10.1177/08959374970110041901
12. Amaechi BT, Higham S (2001) Diagnosis of dental caries using quantitative light-induced fluorescence. Proc SPIE 4432:110–117. https://doi.org/10.1117/12.447125
13. Khosroshahi ME, Taghizadeh Khoi N (2014) Comparison of blue wavelengths and scan velocity effects on the detection of enamel surface caries using steady state laser-induced autofluorescence spectroscopy. J Appl Spectrosc 81:347–354 UDC 621.375.826: (616- 002.4+616.314)
14. Jeon R, Hellen A, Matveinko A, Mandelis A, Abram S, Amaechi B (2007) Detection of interproximal demineralized lesions on human teeth in vitro using frequency-domain infrared photothermal radiometry and modulated luminescence. J Biomed Opt 12:034028. https://doi.org/10.1117/1.2750289
15. Gadalla M, El Sharkawi M (2010) Non-invasive technique for human caries detection and monitoring using time-resolved photothermal imaging. J Med Biol Eng 30:113–118
16. Darling C, Jiao J, Lee C, Kang H (2010) Near-IR polarization imaging of sound and carious dental enamel. Proc SPIE 7549: 75490L. https://doi.org/10.1117/12.849341
17. Hibst R, Papulus R, Lussi A (2001) Detection of occlusal caries by laser fluorescence: basic and clinical investigations. Med Laser Appl 16:205–213. https://doi.org/10.1078/1615-1615-00024
18. Boltzan de Paula A, Campos J, Dinizi M, Hebling J (2011) In situ and in vitro comparison of laser fluorescence with visual inspection

in detecting occlusal caries lesions. Lasers Med Sci 26:1–5. https://doi.org/10.1007/s10103-009-0731-y
19. Jeffery I, Lawerson B, Longbottom C (1991) CO_2 laser application to the mineralized dental tissues. J Dent 18:24–30. https://doi.org/10.1016/0300-5712(90)90247-c
20. Holt RA, Nordquist R (1994) Ho:YAG laser in dentistry: photoconditioning of dentinal surfaces. Proc SPIE 2128:308–318. https://doi.org/10.1117/12.184914
21. White J (1996) Nd:YAG laser transmission through enamel and dentin. Lasers in Dentistry II. Proc SPIE 2672:200–207. https://doi.org/10.1117/12.238769
22. Keller U, Hibst R (1996) Patient's response to cavity preparation using the Er:YAG laser. Proc SPIE 2623:84–87. https://doi.org/10.1117/12.260663
23. Fried D, Featherstone B, Visuri R, Seka W, Walsh J (1996) The caries inhabitation potential of Er:YAG and Er:YSGG laser radiation. Proc SPIE 2672:73–79. https://doi.org/10.1117/12.238755
24. Neev J, Rubenchik A, Staurt B (1996) Ultrashort-pulse laser system for hard dental tissue procedures. Proc SPIE 2672:210–221. https://doi.org/10.1117/12.238770
25. McNally K, Grillines B, Dawes J (1994) Dye-assisted diode laser ablation of carious enamel and dentine. Aust Dent J 44:169–175
26. Jennett E, Motamedi M, Rastgar C, Fredrickson C (1994) Dye-enhanced ablation of enamel by pulsed lasers. J Dental Res 73: 1841–1847. https://doi.org/10.1177/00220345940730120801
27. Esenaliev R, Oraevsky A, Rastgar S, Fredickson C (1996) Mechanism of dye-enhanced pulsed laser ablation of hard tissues: implications for dentistry. IEEE J Quant Elect 2:836–846. https://doi.org/10.1109/2944.577306
28. Prahi S (1999) Optical absorption of indocyanine green (ICG). Oregon Medical Laser Center http://www.omlc.ogi.edu/index.html
29. Al-Dahan Z (2009) Study of a dye-assisted diode laser system for ablation of dental caries. Nahrain Univ College Eng J (NUCEJ) 12: 47–57 https://www.researchgate.net/publication/236012618
30. Chuck R, Oz M, Johnson J, Parangi S (1989) Dye-enhanced laser tissue welding. Lasers Surg Med 9:471–477. https://doi.org/10.1002/lsm.1900090508
31. Khosroshahi ME, Nourbakhsh M, Sarmi S, Hooshyar A (2008) Application of albumin protein and indocyanine green chromophore for tissue soldering using an IR diode laser: ex vivo and in vivo studies. Photomed Laser Surg 723-733. https://doi.org/10.1089/pho.2008.2463
32. Ishimuru A (1978) Wave propagation and scattering in radiative media, vol 1. Academia, NewYork
33. Yoon G, Welch A, Motamedi M, van Germet G (1987) Development and application of three dimensional light distribution model for laser irradiated tissue. IEEE J Quant Elect 23:1721–1733. https://doi.org/10.1109/JQE.1987.1073224
34. Anderson R, Parrish JA Selective photothermolysis: precise microsurgery by selective absorption of pulsed radiation. Science 29: 524–527. https://doi.org/10.1126/science.6836297
35. McNally M, Sorg B, Chan E, Welch A (2000) Optimal parameters for laser tissue soldering. Part I: tensile strength and scanning electron microscopy analysis. Lasers Surg Med 26:346–356. https://doi.org/10.1002/(sici)1096-9101(1999)24:5<319::aid-lsm2>3.0.co;2-n